Stochastic beam dynamics in quasi-isochronous storage rings

M. Bai,[1] D. Jeon,[1] S. Y. Lee,[1] K. Y. Ng,[2] A. Riabko,[1] and X. Zhao[1]
[1]*Department of Physics, Indiana University, Bloomington, Indiana 47405*
[2]*Fermilab, P.O. Box 500, Batavia, Illinois 60510*
(Received 26 August 1996)

We investigate effects of quantum fluctuation, potential well distortion, quantum lifetime, and Touschek lifetime of the quasi-isochronous (QI) dynamical system. The Fokker-Planck equation is employed to study the equilibrium bunch distribution. The quantum lifetime in the moderate damping regime is compared with analytical formulae. The effects of harmonic radio-frequency phase modulation on equilibrium distribution function, quantum lifetime reduction, and the occurrence of stochastic resonance are studied. The formula for the Touschek lifetime for the QI dynamical system is derived and studied. [S1063-651X(97)04002-6]

PACS number(s): 29.20.Dh, 03.20.+i, 05.45.+b

I. INTRODUCTION

Very short electron bunches, e.g., submillimeter in bunch length, can enhance applications such as time resolved experiments, next generation light sources, coherent synchrotron radiations, and damping rings for the next linear colliders [1]. A method to produce short bunches is to reduce the phase slip factor, or the momentum compaction factor α_c for electron storage rings. Because of its potential benefit, the physics of particle dynamics in low α_c lattices is important [2–4].

In our earlier papers [2,3], we studied single particle dynamics and the stability of the quasi-isochronous (QI) dynamical system, where the particle motion satisfies the universal Weierstrass equation (see Appendix A). The particle motion is described by the Weierstrass $\wp$ function or the Jacobian elliptic function [5,6]. We found that the QI dynamical system is not sensitive to the radio-frequency (rf) voltage modulation provided that the modulation amplitude is less than 20%. On the other hand, we showed that the QI dynamical system exhibited chaos at a relatively weak rf phase modulation. Due to the synchrotron radiation damping, stable fixed points (SFPs) of parametric resonances become attractors. As the amplitude of the applied phase modulation increases, the system exhibits a sequence of period-two bifurcations enroute towards global chaos for a modulation tune $\omega_m \in (0,2)$. The sequence of period-two bifurcations has been attributed to parametric resonances of the Hamiltonian system. The critical phase modulation amplitude vs the modulation tune (see Fig. 6 in Ref. [3]) shows a cusp near the transition modulation tune between the 2:1 and the 1:1 parametric resonances.

Electrons in a storage ring emit synchrotron radiations. The synchrotron light frequency spectrum is continuous up to a critical energy given by $\hbar\omega_c = 3\hbar c\gamma^3/2\rho$, where $\hbar$ is Planck's constant, γ is the relativistic Lorentz factor of electrons, c is the speed of light, and ρ is the bending radius. The synchrotron radiation is a quantum mechanical process. Since an electron normally emits hundreds to thousands of photons per revolution and the average energy of each emitted photon is small, the quantum effect of photon emission can be simulated by a white noise. Thus electrons, in the presence of quantum fluctuation, are acted on a Langevin force. Including the harmonic rf noise and the synchrotron radiation damping, the equation of motion for electrons in a QI storage ring is similar to a class of physical problems such as the current biased Josephson junction [7], the stochastic resonance [8], etc.

This paper studies effects of the quantum fluctuation, potential well distortion, and Coulomb scattering leading to the Touschek effect. Section II studies effects of quantum fluctuation on the equilibrium beam distribution and the quantum lifetime in the moderate damping regime. We also study the effect of potential well distortion on the beam distribution function. Section III studies effects of the harmonic rf phase modulation on beam distribution function, diffusion rate enhancement, and the stochastic resonance. Section IV studies the Touschek lifetime limitation. The conclusion is given in Sec. V.

II. QUANTUM FLUCTUATION AND THE LANGEVIN EQUATION

The synchrotron equation of motion for an electron in a QI storage ring, in the presence of quantum fluctuation and harmonic rf phase modulation, is given by (see Appendix A),

$$\frac{d^2x}{dt^2} + A\frac{dx}{dt} + \frac{dU}{dx} = -\omega_m B\cos(\omega_m t + \chi) + D\xi(t). \quad (1)$$

Here $t = \nu_s\theta$ is the time variable, ν_s is the small amplitude synchrotron tune, θ is the particle orbiting angle, A is the phase space damping parameter, ω_m and B are the rf phase modulation tune and amplitude, respectively, and $U = \frac{1}{2}x^2 - \frac{1}{3}x^3$ is the QI potential. The conjugate phase space coordinates $(\phi, -\Delta p/p_0)$ for the synchrotron motion is transformed to the normalized coordinates by

$$x = -\frac{\eta_1}{\eta_0}\frac{\Delta p}{p_0}, \quad p = \frac{\nu_s\eta_1}{h\eta_0^2}\phi.$$

The quantum fluctuation is represented by a Langevin force $D\xi(t)$. Since the time for each quantum emission of photon is much shorter than the relaxation time and successive emissions of photons are independent, the Langevin force can be approximated by a white-noise signal $\xi(t)$ with

$$\langle \xi(t) \rangle = 0, \quad \langle \xi(t)\xi(t') \rangle = \delta(t-t'). \tag{2}$$

Here $\langle \cdots \rangle$ represents an ensemble average. The Gaussian random variable with a zero mean and a δ-function correlation is usually called white noise because its spectral distribution is independent of frequency. Methods of integrating the stochastic differential equation are listed in Appendix B.

In the absence of damping and harmonic rf phase modulation, the unperturbed Hamiltonian is given by

$$H_0 = \frac{p^2}{2} + \frac{1}{2}x^2 - \frac{1}{3}x^3, \tag{3}$$

where the separatrix energy of the Hamiltonian is $E_{sx} = 1/6$.

A. Damping decrement and the damping time

The energy loss per revolution for a particle having an energy offset of ϵ with respect to the synchronous particle is given by

$$U(\epsilon) \approx U_0 + \epsilon U'. \tag{4}$$

Here U_0 is the average energy loss per revolution for the synchronous particle and U' is the slope of the energy loss with respect to particle energy. Normally, the energy variation U' is small, i.e.,

$$U' = \frac{U_0 J_E}{E_0} \ll 1, \tag{5}$$

where E_0 is the energy of the synchronous particle, and J_E is the damping partition number.

The average energy loss of the synchronous particle can be compensated by the energy gain in rf cavities. Thus the change of the particle energy offset in a complete revolution is given by

$$\epsilon' = \epsilon - U'\epsilon - W, \tag{6}$$

where W depicts the Wiener process of Eq. (B2) due to quantum fluctuation in the photon emission. Averaging over many revolutions, we have

$$\frac{d}{d\theta}\langle \epsilon \rangle = -\frac{U'}{2\pi}\langle \epsilon \rangle = -\lambda \langle \epsilon \rangle. \tag{7}$$

Here the damping decrement λ, given by

$$\lambda = \frac{U_0 J_E}{2\pi E_0} \tag{8}$$

is of the order of $10^{-5} - 10^{-3}$ in electron storage rings. In the normalized coordinate, the enhanced damping parameter for QI storage rings becomes

$$A = \frac{\lambda}{\nu_s}. \tag{9}$$

The damping parameter A for QI storage rings is of the order of 0.1–0.5. In the normalized time coordinate, the damping time is given by $t_d = 1/A$.

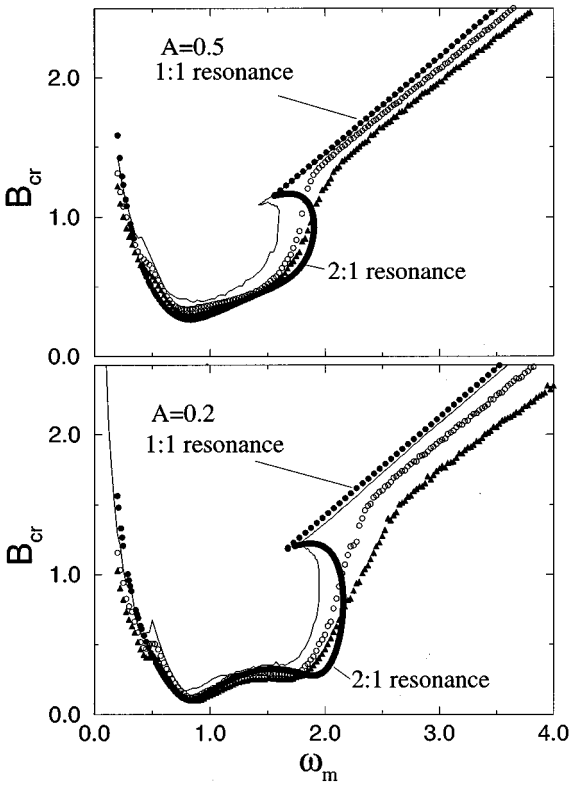

FIG. 1. The critical phase modulation amplitude B_{cr} (thin solid lines) obtained from numerical simulations is shown as function of ω_m for $A = 0.2$ (bottom plot) and $A = 0.5$ (top plot). Circle dots are $B_{cr,1:1}$ and $B_{2:1}$ for the 1:1 and 2:1 parametric resonances. Note that the cusp in B_{cr} obtained from numerical simulations is due to the transition from the 2:1 to the 1:1 parametric resonances. Including the quantum diffusion, the critical phase modulation amplitude B_{cr} is reduced, where B_{cr} for $D = 0.03$ (open circles) and $D = 0.05$ (solid triangles) are obtained by numerically integrating the stochastic differential equation.

B. Stability limit of stochastic dynamical system

Without quantum fluctuation, the stability limit of the QI dynamical system is determined mainly by the 1:1 and 2:1 parametric resonances, which correspond to the dipole and quadrupole modes respectively (see Fig. 6 in [3]). Including white noise, we expect that resonance islands will be smeared and the global chaos will be enhanced. Figure 1 shows the critical modulation parameter B_{cr} as a function of the modulation frequency ω_m for $A = 0.2$ (bottom) and $A = 0.5$ (top) respectively. Note that the white noise with $D = 0.03$ (open circles) and $D = 0.05$ (solid triangles) has effectively smoothed the cusp near $\omega_m \approx 2$ resulting from the 1:1 and 2:1 parametric resonances (solid circles). Furthermore, the quantum fluctuation can effectively reduce the parametric space where the period-two bifurcation occurs. In other words, quantum fluctuation enhances the onset of global chaos.

C. Fokker-Planck equation

The Kramer-Smoluchowski-Fokker-Planck (KSFP) or simply the Fokker-Planck equation for distribution function Ψ associated with the Langevin equation of Eq. (1) is given by [9,10]

$$\frac{\partial \Psi}{\partial t} = \left[-p\frac{\partial}{\partial x} + A\frac{\partial}{\partial p}p + (x-x^2)\frac{\partial}{\partial p} + \frac{D^2}{2}\frac{\partial^2}{\partial p^2} + B\omega_m \sin(\omega_m t+\phi)\frac{\partial}{\partial p}\right]\Psi. \quad (10)$$

In case of zero harmonic modulation with $B=0$, the normalized steady-state distribution function for the Langevin equation is given by

$$\Psi(E) = \frac{1}{E_{\rm th}} e^{-H_0/E_{\rm th}} = \frac{1}{E_{\rm th}} e^{-E/E_{\rm th}}, \quad (11)$$

where the *energy* E is a Hamiltonian value, and the ''thermal'' energy $E_{\rm th}$ is given by the Einstein relation, or the fluctuation-dissipation theorem

$$E_{\rm th} = \frac{D^2}{2A}. \quad (12)$$

It is worth noting that the isodensity contour of distribution function follows the equienergy line of the unperturbed Hamiltonian.

The normalization of Eq. (11) is correct only in a small bunch limit where $E_{\rm th}$ is small. If a beam bunch contains N particles, the distribution function becomes

$$\frac{dN}{dE} = \frac{N}{E_{\rm th}} e^{-E/E_{\rm th}}. \quad (13)$$

Using Eq. (3) for the unperturbed Hamiltonian, the distribution function is Gaussian in the small bunch approximation where $E_{\rm th}$ is small. Since the rms momentum spread for a small electron bunch is given by

$$\left(\frac{\sigma_p}{p_0}\right)^2 = C_q \frac{\gamma^2}{J_E \rho} \quad (14)$$

for an isomagnetic storage ring, where ρ is the bending radius, $C_q = 3.84\times 10^{-13}$ m, and J_E is the damping partition number, the diffusion parameter is given by

$$D = \sqrt{\frac{2AC_q}{J_E\rho}}\left|\frac{\eta_1}{\eta_0}\right|\gamma. \quad (15)$$

Here the quantum fluctuation coefficient D of the QI dynamical system is also enhanced by the smallness of $|\eta_0|$. In fact, if the ratio $|\eta_1/\eta_0|$ were not properly compensated, the thermal energy parameter $D^2/2A$ would also be enhanced.

To verify the distribution function of Eq. (13), stochastic integration methods are applied to solve the Langevin equation. Some algorithms used in particle beam simulations for stochastic differential equation are listed in Appendix B. All numerical algorithms give similar results with an equilibrium distribution given by Eq. (11). For example, Fig. 2 shows a final equilibrium distribution function obtained from numerical tracking with the random walk algorithm performed according to Eq. (B2) with parameters $2\pi\nu_s = 0.05$, $A=0.1$, and $D=0.056\,568\,54$. We track 10 000 particles, randomly distributed initially in a rectangle with $|p|<1/(2\sqrt{3})$ and $-1/4<x<1/2$, for 1×10^6 turns. The ''energy'' within the QI bucket is divided into 200 bins with a bin size of

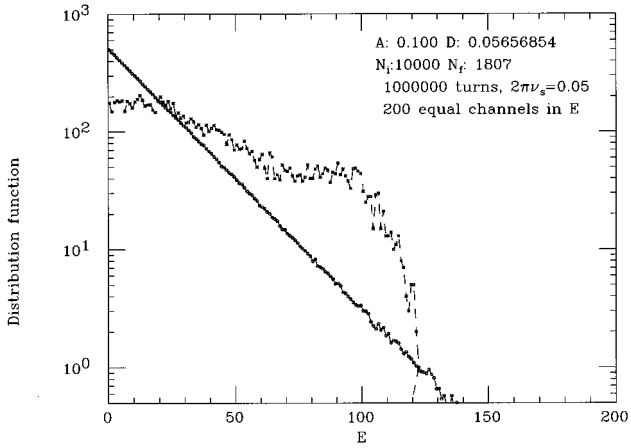

FIG. 2. The solid line shows the equilibrium distribution function $\Psi(E)$ obtained from the numerical simulation using random walk algorithm discussed in Appendix B. Our results verify the validity of the analytic solution of Eq. (11). The dashed shows the initial distribution function used in our numerical simulation. Other stochastic integration methods yield similar results.

$\Delta E = 1/1200$ each. Statistically, there would be 50 particles per bin with a statistical fluctuation of $\sqrt{50}=7.07$ particles. With our chosen damping parameter $A=0.1$, particles fall into their steady-state distribution very fast, equilibrium distribution functions can be recorded every 2000 turns. At the end of a tracking run, 500 distributions are averaged to reduce the average statistical fluctuation to 0.32 particle in each energy bin. After every turn, we also record number of particles lost and increased the weight of surviving particles accordingly when they were assigned to various energy bins. In this way, distribution functions of every 2000 turns can be averaged with equal weight.

The semilogarithmic plot of particle populations vs the energy bin shown in Fig. 2 indicates that the distribution is exponential, represented by Eq. (13). The rms energy $E_{\rm th}$ of the bunch can be obtained from the slope or the intercept of the distribution function at the zero energy bin. From the slope of the straight line in Fig. 2, we determine $E_{\rm th}=0.0164$, which agree very well with the expected value of $E_{\rm th}=D^2/(2A)=0.0160$. The value of $E_{\rm th}$ obtained from numerical simulations is shown as circles in Fig. 3. The theoretical value of Eq. (12) is shown as the dotted line.

It is worth pointing out that the synchrotron tune does not affect the steady-state distribution. However, it must be chosen to be small enough so that there are a sufficiently large number of random excitations during one synchrotron period. In our tracking example with $2\pi\nu_s=0.05$, there are about about 125.7 steps of random walk in one synchrotron period. Further reduction in $2\pi\nu_s$ does not lead to any difference in tracking results.

Figure 4 shows the equilibrium distribution function obtained from numerical simulations of 5000 particles with $A=0.2$ and $D=0.113\,137\,08$. The solid line marks the separatrix of the unperturbed Hamiltonian. The dotted line marks a torus of the unperturbed Hamiltonian with an energy $E=2E_{sx}$. We note particularly that the phase space distortion shown in Fig. 3 of Ref. [2] is effectively compensated by the stochastic process. There are slightly more particles

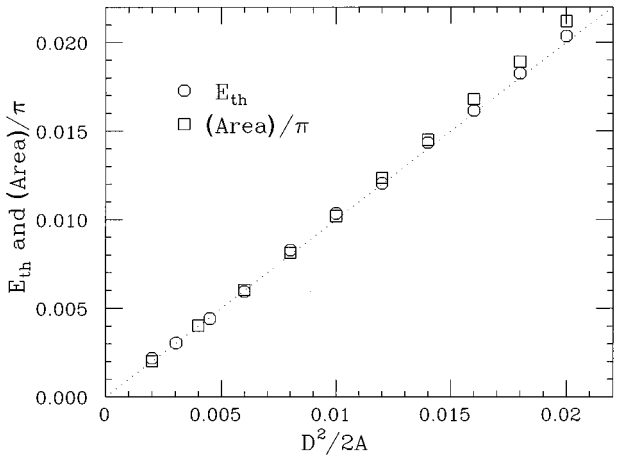

FIG. 3. The rms energy of the equilibrium distribution function E_{th} obtained from numerical integration of stochastic integral equation is compared with the theoretical value of $D^2/2A$ (dotted line) derived from the Fokker-Planck equation. The rms phase space area, divided by π, is shown for comparison.

outside the separatrix with $p>0$. This is due to the fact that particle loss will follow closely the Hamiltonian trajectory. The equilibrium distribution functions are identical for all dynamical systems with identical thermal energy E_{th}. However, we will show that the quantum lifetime depends also on the damping parameter A.

The rms phase space area $\mathcal{A}$ of the beam distribution is given by

$$\frac{\mathcal{A}}{\pi}=\sqrt{\mathrm{var}(x)\mathrm{var}(p)-[\mathrm{covar}(x,p)]^2}, \tag{16}$$

where

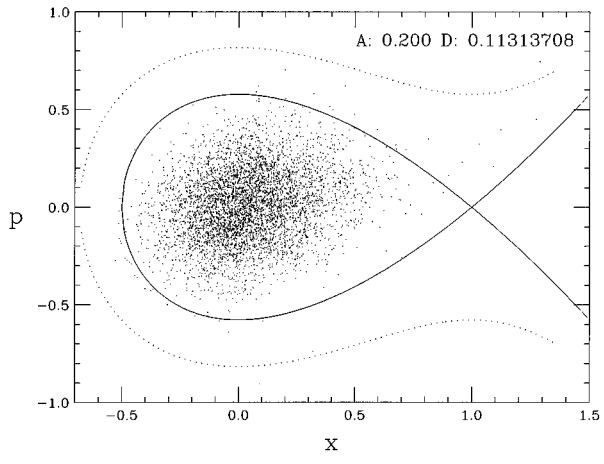

FIG. 4. The equilibrium distribution function in the (x,p) phase space obtained from the numerical simulation of 5000 particles with $A=0.2$ and $D=0.113\,137\,08$. The plot is used to demonstrate that the distribution function follows the contour of the *unperturbed Hamiltonian*. The separatrix is shown as the solid line. The dotted line shows the Hamiltonian contour with an energy that is equal to two times of the separatrix energy. The phase space distortion due to the damping is compensated by the quantum diffusion.

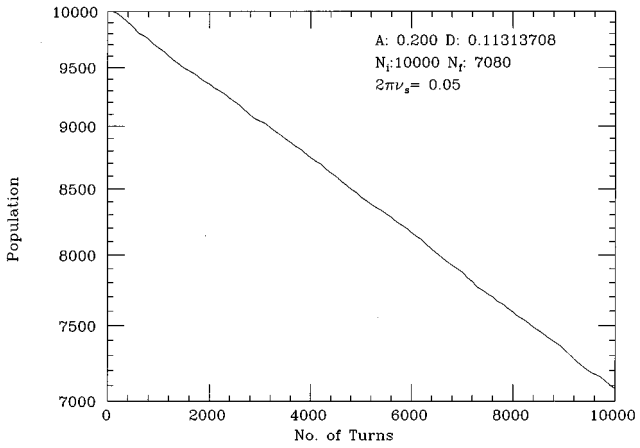

FIG. 5. The number of surviving particles vs time in number of turns. The slope of the exponential decay rate is called the quantum lifetime.

$$\mathrm{var}(x)=\langle(x-\langle x\rangle)^2\rangle,$$

$$\mathrm{var}(p)=\langle(p-\langle p\rangle)^2\rangle,$$

$$\mathrm{covar}(x,p)=\langle xp\rangle-\langle x\rangle\langle p\rangle.$$

Here $\langle\cdots\rangle$ denotes an average over the beam distribution. In a small bunch approximation, the rms phase space area is equal to πE_{th}. Rectangle symbols in Fig. 3 show the rms phase space area obtained from numerical simulations. The agreement of $\mathcal{A}/\pi$ with E_{th} indicates that the distribution is nearly Gaussian in a small bunch approximation.

D. Quantum lifetime

The steady-state distribution, such as Eq. (13), arises from an equilibrium process between synchrotron radiation damping and quantum excitation. This means that at any contour of energy E, the particle flux leaving the contour as a result of quantum excitation is balanced by a flux entering the contour due to damping.

In reality, particles inside the bucket can escape the potential barrier due to the Langevin force. In a quasisteady state, the form of distribution function in phase space does not depend on the number of particles, which decreases with time. Thus the flux that leaves the dynamical aperture is given by

$$\left.\frac{dN(t)}{dt}\right|_{E_1}=-\frac{N(t)}{\tau_q}, \tag{17}$$

where τ_q is the *quantum lifetime*, and E_1 is the dynamical aperture. In a small damping limit, E_1 is approximately equal to the separatrix energy E_{sx} of the unperturbed Hamiltonian. Figure 5 shows the number of surviving particles, obtained from a numerical simulation, as a function of the turn number. We find that the particle number decays exponentially with time. Although the quantum lifetime in storage rings is usually much longer than the lifetime limitation arising from processes such as the beam gas scattering, the intrabeam scattering, the Touschek lifetime, etc., the general properties

of the quantum lifetime for the QI dynamical system with a moderate damping, i.e., $A \geqslant 0.01$, is not well known in accelerator physics. Furthermore, this particular dynamical system is also important to other branches of physics [11].

1. Quantum lifetime in the small damping limit

In the small damping limit, the Hamiltonian contour is not greatly distorted. When a particle crosses the separatrix, it is likely to escape the potential barrier. The quantum lifetime can be obtained by using the condition of flux conservation.

The flux that enters the contour $E=E_1$ at any time t is given by

$$\left.\frac{dN(t)}{dt}\right|_{E_1} = \left.\frac{dN(E,t)}{dE}\right|_{E_1} \left.\frac{dE}{dt}\right|_{E_1}, \tag{18}$$

where dN/dE is given by Eq. (13), and the damping rate dE/dt can be obtained from integrating Eq. (1) with

$$\left.\frac{dE}{dt}\right|_{E_1} = -A\left\langle \left(\frac{dx}{dt}\right)^2 \right\rangle \approx -AE_1. \tag{19}$$

Here the equipartition theorem is used to obtain the last approximate identity (see Appendix C). Substituting Eqs. (19) and (13) into Eq. (18), the quantum lifetime of the bunch is given by

$$t_q = \frac{E_{\rm th}}{AE_1} e^{E_1/E_{\rm th}}, \tag{20}$$

or

$$\tau_q = \frac{E_{\rm th}}{2\pi\nu_s AE_1} e^{E_1/E_{\rm th}} \text{ turns}, \tag{21}$$

which is inversely proportional to the damping parameter A. This formula is commonly used in estimating the quantum lifetime for nominal non-QI electron storage rings, where the parameter A is small.

Figure 6 shows the quantum lifetime obtained from numerical simulations vs damping parameter A for a constant $E_{\rm th}=0.038\,72$. The solid line in Fig. 6 shows the quantum lifetime calculated from Eq. (21) with $E_1=E_{sx}$. This result agrees reasonably well with that obtained from numerical simulations only at a small damping limit with $A \leqslant 0.01$. The quantum lifetime is considerably larger than the prediction of Eq. (21) at a medium damping with $A \geqslant 0.01$. This can be understood by the fact that the effective bucket area for a moderate damping system is larger than that of a weak damping system.

2. Lifetime for moderate damping systems

Kramers [12] and Chandrasekhar [13] derived a formula for the particle escaping lifetime in moderate damping regime given by

$$\tau_{q,\rm KC} = \left[\left(1+\frac{A^2}{4\omega_{\rm UFP}^2}\right)^{1/2} + \frac{A}{2\omega_{\rm UFP}}\right]\frac{2\pi}{\omega_{\rm SFP}} e^{E_1/E_{\rm th}}, \tag{22}$$

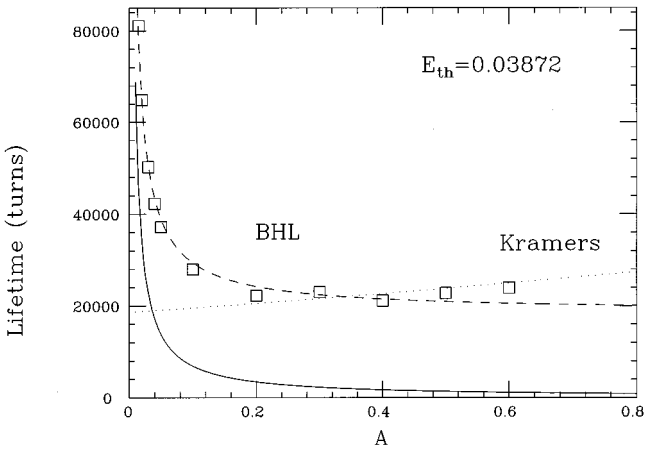

FIG. 6. The quantum lifetime in number of revolutions obtained from numerical simulations is plotted vs the damping parameter A for a fixed $E_{\rm th}=0.038\,72$. The solid line shows the theoretical estimate of a weak damping limit, the dotted line shows the theoretical estimate of Kramers's formula, and the dashed line shows the theoretical value of the BHL formula.

where $\omega_{\rm SFP}$ is the natural frequency of the potential at the SFP, and $\omega_{\rm UFP}$ is the imaginary frequency at the UFP. The dotted line shown in Fig. 6 shows the Kramers's moderate damping lifetime, which depends slowly on A.

3. BHL formula

Büttiker, Harris, and Landauer (BHL) [11] studied the extremely underdamped Josephson-junction circuit and found a lifetime formula for thermal excitation given by

$$\tau_{q,\rm BHL} = \frac{[(1+4E_{\rm th}/AfE_1)^{1/2}+1]^2}{4}\frac{2\pi}{\omega_{\rm SFP}} e^{E_1/E_{\rm th}}. \tag{23}$$

Here $f=7.2$ is the factor relating the separatrix energy to the separatrix action for the QI dynamical system. The BHL formula reduces to Eq. (21) in the small damping limit with a linear oscillator approximation where $f=2\pi$. The dashed line marked BHL in Fig. 6 provides a fair agreement with that obtained from numerical simulations.

E. Potential well distortion

Particle motion in a storage ring is also affected by the wake field generated by the circulating beam. The energy equation is given by

$$\frac{d\delta}{d\theta} = \frac{eV_0\cos\phi_s}{2\pi\beta^2 E}\phi - \frac{e^2 N}{2\pi\beta^2 E}\int_{-\infty}^{\tau} d\tau'\rho(\tau')W(\tau-\tau'). \tag{24}$$

Here τ is the real time coordinate related to the particle rf phase coordinate ϕ by

$$\tau = -\frac{\phi}{h\omega_0}, \tag{25}$$

$\rho(\tau)$ is the density of the beam bunch with the normalization

$$\int \rho(\tau)d\tau = 1,$$

N is the number of particles in a bunch, and the wake function $W(\tau)$ is related to the impedance $Z_{\parallel}(\omega)$ by

$$W(\tau) = \frac{1}{2\pi}\int_{-\infty}^{\infty} e^{j\omega\tau} Z_{\parallel}(\omega)d\omega. \tag{26}$$

Using normalized coordinates x,p (see Appendix A) and the time coordinate $t=\nu_s\theta$, Eq. (24) becomes

$$\frac{dx}{dt} = p - \frac{e^2N}{2\pi\beta^2E}\frac{\eta_1}{\eta_0\nu_s}\int_p^{\infty} d\widetilde{p}\,\widetilde{\rho}(\widetilde{p})W\left(\frac{\eta_0^2}{\eta_1\omega_0\nu_s}[\widetilde{p}-p]\right), \tag{27}$$

where

$$\widetilde{\rho}(\widetilde{p}) = \frac{\eta_0^2}{\omega_0\nu_s\eta_1}\rho\left(\frac{\eta_0^2}{\omega_0\nu_s\eta_1}\widetilde{p}\right)$$

is the normalized distribution function with $\int\widetilde{\rho}(y)dy=1$. The corresponding effective Hamiltonian for orbiting particles becomes

$$H_{\text{eff}} = \frac{p^2}{2} + \frac{x^2}{2} - \frac{x^3}{3} - \frac{e^2N}{2\pi\beta^2E}\frac{\eta_1}{\eta_0\nu_s} \times \int_{-\infty}^{p} d\overline{p}\int_{\overline{p}}^{\infty} d\widetilde{p}\,\widetilde{\rho}(\widetilde{p})W\left(\frac{\eta_0^2}{\eta_1\omega_0\nu_s}[\widetilde{p}-\overline{p}]\right). \tag{28}$$

When both white noise and phase space damping are included, the equilibrium distribution function becomes

$$\Psi(x,p) = \mathcal{N}e^{-H_{\text{eff}}/E_{\text{th}}}, \tag{29}$$

where $\mathcal{N}$ is the normalization factor determined by

$$\int \Psi(x,p)dxdp = 1.$$

Letting $\widetilde{\rho}(p)=\int\Psi(x,p)dx$, we obtain the Haissinski equation [14]

$$\widetilde{\rho}(p) = C\exp\left\{-\frac{1}{E_{\text{th}}}\left[\frac{p^2}{2} - \frac{e^2N}{2\pi\beta^2E}\frac{\eta_1}{\eta_0\nu_s} \times \int_{-\infty}^{p} d\overline{p}\int_{\overline{p}}^{\infty} d\widetilde{p}\,\widetilde{\rho}(\widetilde{p})W\left(\frac{\eta_0^2}{\eta_1\omega_0\nu_s}[\widetilde{p}-\overline{p}]\right)\right]\right\}, \tag{30}$$

where C is a self-consistent normalization constant. A self-consistent solution to the Haissinski equation can provide an equilibrium distribution function to the dynamical system.

For simple wake field model with a resistive broadband or an inductive broadband impedance, the distribution function can be derived from analytic formulae [15]. Recent numerical calculations for the potential well distortion for the QI storage rings [16] shows that when the bunch area is small, i.e., small E_{th}, the effect of potential well distortion is similar to that of the normal rf system.

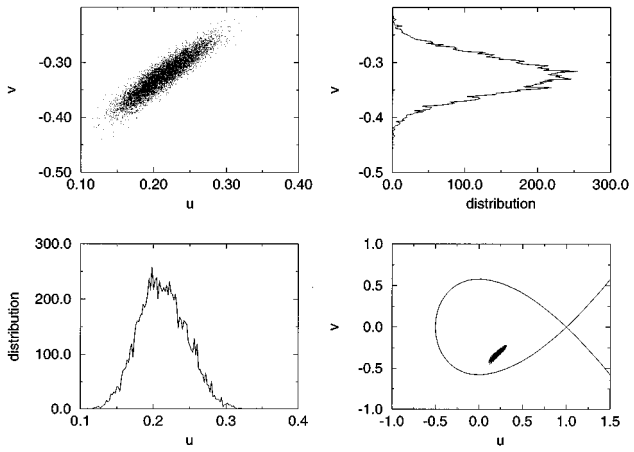

FIG. 7. The top-left plot shows the equilibrium distribution function at a Poincaré surface of section with parameters $A=0.2$, $B=0.4$, $\omega_m=2.1$, and $D=0.009$. The projection of the equilibrium distribution function onto the u and v axes are shown, respectively, in the bottom-left and top-right plots. The bottom-right plot shows the relative position of the beam bunch in the QI bucket.

III. EFFECTS OF THE HARMONIC RF PHASE MODULATION

Neglecting quantum fluctuation, the attractor solution arising from the rf harmonic phase modulation for the 1:1 parametric resonance can be obtained by the harmonic linearization method with [2,3]

$$x = X_0 + X_1\cos(\omega_m t + \alpha), \tag{31}$$

where X_0, X_1, and α are determined by the solutions of following equations:

$$\omega_m^2B^2 = A^2\omega_m^2X_1^2 + (\omega_m^2 - \sqrt{1-2X_1^2})^2X_1^2,$$

$$X_0 = \frac{1}{2}(1-\sqrt{1-2X_1^2}),$$

$$\tan\alpha = \frac{-A\omega_m}{\omega_m^2 - \sqrt{1-2X_1^2}}.$$

Figure 8 of Ref. [2] shows characteristic properties of X_1, which corresponds to the SFP of the 1:1 parametric resonance.

When the effects of quantum fluctuations are included, we expand the phase space coordinate around the attractor solution with

$$x = X_0 + X_1\cos(\omega_m t + \alpha) + u. \tag{32}$$

The equation of motion for the coordinate u becomes

$$u'' + Au' + [\sqrt{1-2X_1^2} - 2X_1\cos(\omega_m t+\alpha)]u - u^2 = D\xi(t). \tag{33}$$

The equivalent local Hamiltonian around the SFP is given by

$$H_{1:1} = \frac{1}{2}u'^2 + \frac{1}{2}[\sqrt{1-2X_1^2} - 2X_1\cos(\omega_m t+\alpha)]u^2 - \frac{1}{3}u^3, \tag{34}$$

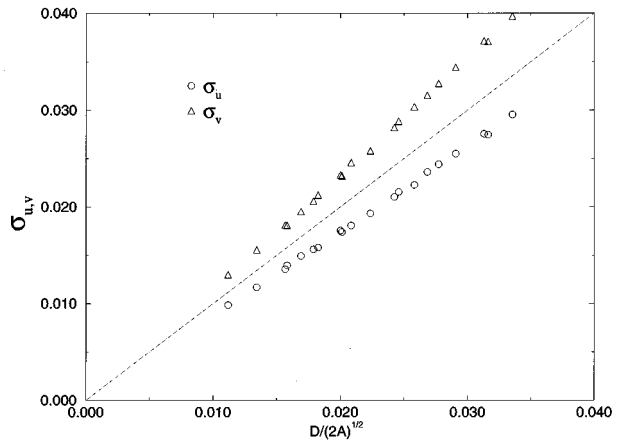

FIG. 8. The rms widths σ_v and σ_u of the projected distribution function for $B=0.4$ and $\omega_m=2.1$ are plotted as a function of $D/\sqrt{2A}$. Note here that the geometric means of the rms widths is nearly equal to $D/\sqrt{2A}$, i.e., the equilibrium distribution function follows the potential energy contour of the resonance island with a thermal energy parameter given by $E_{\rm th}$.

where the potential well around the SFP of the 1:1 parametric resonance is essentially similar to the original Hamiltonian with a spring constant that depends on the amplitude X_1 and time t. The time dependent harmonic modulation in the spring constant becomes the source of the Mathieu instability [17–19]. This provides the mechanism for the first period-two bifurcation leading to global chaos in the QI dynamical system.

A. Equilibrium distribution function

The Fokker-Planck equation associated with the Langevin equation (33) for distribution function $\Psi(u,v,t)$, where $v=u'$, is given by

$$\frac{\partial\Psi}{\partial t}=\left[L_0-\frac{\partial}{\partial v}[2X_1\cos(\omega_m t+\alpha)u]\right]\Psi. \tag{35}$$

Here L_0 is the time independent differential operator given by

$$L_0=-\frac{\partial}{\partial u}v+\frac{\partial}{\partial v}(Av+\sqrt{1-2X_1^2}u-u^2)+\frac{D^2}{2}\frac{\partial^2}{\partial v^2}.$$

The solution of time independent Fokker-Planck equation

$$\frac{\partial\Psi_0}{\partial t}=L_0\Psi_0 \tag{36}$$

is given by

$$\Psi_0=\frac{1}{E_{\rm th}}\exp\left(-\frac{1}{E_{\rm th}}\left[\frac{v^2}{2}+\frac{\sqrt{1-2X_1^2}}{2}u^2-\frac{1}{3}u^3\right]\right). \tag{37}$$

Note here that the potential well around the SFP of the 1:1 parametric resonance for the QI Hamiltonian is lowered by the attractor solution amplitude X_1. When the attractor amplitude reaches $X_1=1/\sqrt{2}$, the potential well disappears [2,3], and the QI dynamical system becomes globally unstable. It is worth pointing out that the equilibrium rms beam width, even in the presence of harmonic rf phase modulation, is essentially determined by the parameter $E_{\rm th}$ of Eq. (12) alone.

To solve time dependent Fokker-Planck equation of Eq. (35), we express the solution as $\Psi=\Psi_0 g$ to obtain

$$\begin{aligned}\frac{\partial g}{\partial t}&=L_0 g+D^2\left(\frac{1}{\Psi_0}\frac{\partial\Psi_0}{\partial v}\right)\frac{\partial g}{\partial v}-[2X_1\cos(\omega_m t+\alpha)u]\\&\quad\times\left(\frac{1}{\Psi_0}\frac{\partial\Psi_0}{\partial v}g+\frac{\partial g}{\partial v}\right)\\&\approx\left[-v\frac{\partial}{\partial u}+\frac{\partial}{\partial v}(Av+\sqrt{1-2X_1^2}-u^2)+\frac{D^2}{2}\frac{\partial^2}{\partial v^2}\right.\\&\quad\left.-2Av\frac{\partial}{\partial v}+\frac{2X_1uv}{E_{\rm th}}\cos(\omega_m t+\alpha)\right]g.\end{aligned} \tag{38}$$

The top left plot of Fig. 7 shows the steady state distribution function at a Poincaré surface of section obtained from a numerical simulation with parameters $A=0.2$, $B=0.4$, $\omega_m=2.1$, and $D=0.009$. If the attractor amplitude is small, the equilibrium distribution function follows the potential energy contour of the 1:1 parametric resonance island. The projected distribution functions onto u and v axes are plotted on the top-right and bottom-left plots, respectively. The bottom-right plot shows the relative position of the Poincaré surface of section in the QI bucket.

The rms widths σ_u and σ_v of the projected distribution functions obtained from numerical simulations are shown as a function of $D/\sqrt{2A}$ in Fig. 8. Because the equilibrium bunch profile may follow the local potential well of the attractor, the actual rms widths σ_u and σ_v depend on the time for the Poincaré surface of section. In all cases, we find that the rms widths are nearly equal to $D/\sqrt{2A}$ predicted by the solution [Eq. (37)] of Fokker-Planck equation.

It should be pointed out that the attractor solution $x=X_0+X_1\cos(\omega_m t+\alpha)$ is valid only for the attractor solution associated with the 1:1 parametric resonance. In the case of period-2 bifurcation, the attractor solution is given by

$$x=X_0+X_1\cos(\omega_m t+\alpha)+X_{1/2}\cos\left(\frac{1}{2}\omega_m t+\beta\right), \tag{39}$$

and consequently the equilibrium distribution function $\Psi(u,v,t)$ is modified accordingly. Particles are distributed around around the SFPs of the 2:1 parametric resonance. Because the potential well of the 2:1 parametric resonance is shallow, it can easily be destroyed by the quantum diffusion.

B. Enhancement of quantum diffusion rate due to rf harmonic modulation

When a harmonic modulation is applied, particles are distributed around SFPs, which coherently rotate about the center of the bucket at the modulation tune. The equivalent local potential for particle motion around the SFP is given by [see Eq. (34)]

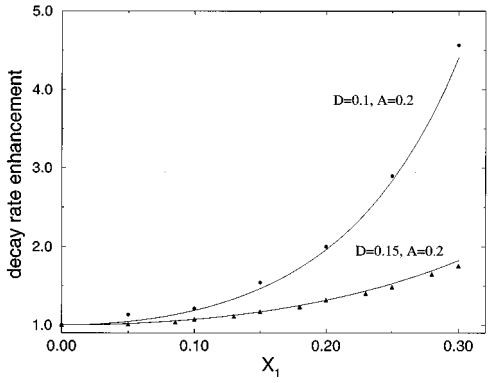

FIG. 9. The triangles and dots show the escape rate enhancement as a function of the attractor amplitude X_1 for $A=0.2$, $D=0.1$, and $D=0.15$. The solid lines are obtained from the BHL formula with E_1 replaced by the separatrix energy $\Delta V_{\rm sep}$ of Eq. (42). The parameter B is varied to obtain appropriate X_1 for a given modulation tune $\omega_m=4$.

$$V(u)=\frac{1}{2}[\sqrt{1-2X_1^2}-2X_1\cos(\omega_m t+\alpha)]u^2-\frac{1}{3}u^3. \tag{40}$$

If the modulation tune is high, e.g., $\omega_m \gg 2$, and if the escape time is much longer than the modulation period, the escaping particle experiences many cycles of the rapid oscillating potential, which can be averaged to obtain an effective potential [20]

$$V_{\rm eff}(u)=\frac{1}{2}\left(\sqrt{1-2X_1^2}+\frac{2X_1^2}{\omega_m^2-\sqrt{1-2X_1^2}}\right)u^2-\frac{1}{3}u^3. \tag{41}$$

The effective potential energy difference between the UFP and the SFP is given by

$$\Delta V_{\rm sep}=\frac{1}{6}\left(\sqrt{1-2X_1^2}+\frac{2X_1^2}{\omega_m^2-\sqrt{1-2X_1^2}}\right). \tag{42}$$

In the presence of the high frequency modulation, the quantum lifetime is given by Eq. (20) or (23) with the separatrix energy E_1 replaced by the potential energy difference $\Delta V_{\rm sep}$. Here, the quantum lifetime reduces to Eq. (20) for $X_1 \to 0$.

Figure 9 shows the enhancement of the particle decay rate, defined as

$$r=\frac{\tau_q}{\tau_{q,m}}, \tag{43}$$

as a function of the amplitude of the SFP X_1 for the modulation tune $\omega_m=4$ and $A=0.2$ with $D=0.1$ (circles) and $D=0.15$ (triangles), respectively. The attractor amplitude X_1 is obtained by varying the parameter B. Solid lines shown in Fig. 9 are theoretical results of Eq. (43) based on the BHL lifetime formula of Eq. (23) with the effective separatrix energy E_1 replaced by $\Delta V_{\rm eff}$ of Eq. (42).

At a low modulation frequency, the coherent beam motion is slow in the QI bucket. Thus particle loss occurs mainly when the potential energy difference between the SFP and the UFP is small, where parametric resonances can greatly enhance the particle loss rate. In this case, using the time averaged separatrix energy $\Delta V_{\rm sep}$ of Eq. (42) for the separatrix energy E_1 in Eq. (23) does not provide a good approximation to the lifetime. A phenomena called *stochastic resonance* will be discussed as follows.

C. Stochastic resonances

When a low frequency harmonic modulation and a white noise are simultaneously applied to this dynamical system, the transition or the decay rate exhibits time dependent periodic enhancement. The period of transition rate enhancement is equal to the period of the harmonic modulation. This periodic enhancement phenomenon is usually called the *stochastic resonance*. Occasionally, this type of enhancement may occur in a stochastic dynamical system with an algorithm of white noise that is not sufficiently random. In this section, we will show that the stochastic resonance arises from the parametric resonance of the low frequency harmonic modulation.

We have shown that a low frequency modulation with a small amplitude modulation induces mainly the 1:1 parametric resonance. Particles incoherently damp to SFPs of the 1:1 parametric resonance. These SFPs rotate about the center of the bucket at the modulation frequency. Below the bifurcation frequency, there are supposedly two islands associated with the 1:1 parametric resonance. However, the outer island is destroyed by overlapping resonances near the separatrix.

Including a Langevin force with white noise, particles are distributed around the SFP with an rms beam width given by the thermal energy $E_{\rm th}$. Since the beam bunch coherently rotates around the center of the bucket, we expect that the particle escape rate $(1/\tau_q)$ will be greatly enhanced when the SFP is near the UFP. The effective potential energy difference between the time dependent SFP and UFP is given by

$$\Delta V_{\rm sep}^{\rm sr}(u)=\frac{1}{6}[\sqrt{1-2X_1^2}-2X_1\cos(\omega_m t+\alpha)]. \tag{44}$$

The upper plot of Fig. 10 shows the particle escape rate obtained from a numerical simulation as a function of time with parameters $2\pi\nu_s=0.04$, $A=0.1$, $B=0.5$, $\nu_m=0.2$, and $D=0.075$. Note here that there are major peaks separated by $\Delta N=1/(\nu_m\nu_s)$ turns. The solid line in the top plot shows the time dependent decay rate of the BHL formula with E_1 replaced by $\Delta V_{\rm sep}$ of Eq. (44). The lower plot of Fig. 10 shows the phase

$$\langle\Phi\rangle=\arctan\left(\frac{\langle p\rangle}{\langle x\rangle}\right)$$

of the centroid of the beam bunch as a function of time. It is clear that when the centroid of the beam bunch is near the UFP, particle loss is greatly enhanced. The occurrence of the periodic beam loss can therefore be associated with the enhancement due to the 1:1 parametric resonance.

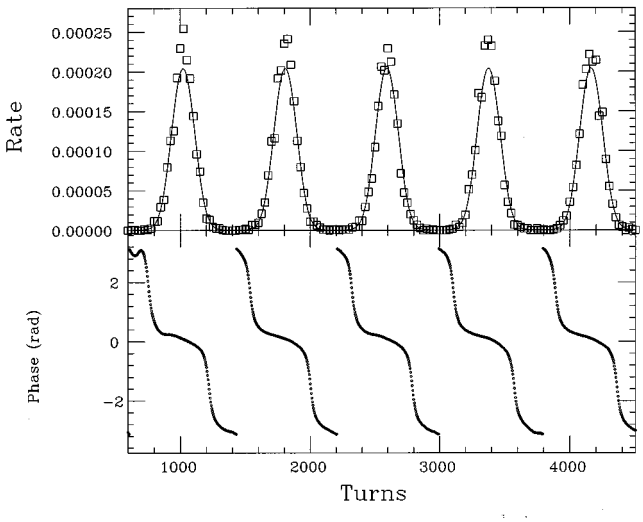

FIG. 10. The upper plot shows the particle escape rate $(1/\tau_q)$ plotted as a function of the turn numbers for parameters $2\pi\nu_s=0.04$, $A=0.1$, $B=0.5$, $\omega_m=0.2$, and $D=0.075$. The solid line shows the escape rate with the BHL formula by substituting E_1 with the separatrix energy of Eq. (44). The lower plot shows the phase of the centroid of the beam bunch. Here we note that the periodic enhancement, called stochastic resonance, of the escape rate is well correlated with the condition that the centroid of the beam bunch is near the UFP of the QI bucket.

IV. TOUSCHEK LIFETIME

In the beam moving frame (BMF), the deviation of the momentum Δp_c of a particle from that of the synchronous particle, which has zero momentum, is related to the momentum deviation in the laboratory frame Δp by

$$\Delta p_c=\frac{1}{\gamma}\Delta p. \tag{45}$$

Thus the momentum deviation in the rest frame of the beam is reduced by the relativistic factor γ. Due to the synchrotron radiation damping and the quantum fluctuation, the rms momentum spread of the beam in the BMF satisfies the following characteristic property

$$\langle (x'_\beta)^2\rangle^{1/2}\gg\langle (z'_\beta)^2\rangle^{1/2}\approx\left\langle\left(\frac{\Delta p_c}{p_0}\right)^2\right\rangle^{1/2}, \tag{46}$$

where x_β, and z_β are betatron coordinates, $x'_\beta=dx_\beta/ds$, $z'_\beta=dz_\beta/ds$ are the slopes of the horizontal and the vertical betatron oscillations, and p_0 is the momentum of the synchronous particle. Since the transverse horizontal momentum spread of the beam is much larger than the momentum spread of the beam in the longitudinal plane, large angle Coulomb scattering can transfer the radial momentum to the longitudinal plane and causes beam loss. This process was first pointed out by Touschek *et al.* in the Frascati e^+e^- storage ring (AdA) [21]. The Touschek effect has been found to be important to many low emittance synchrotron radiation facilities. It may be more important in QI storage rings, where the momentum aperture is determined by the momentum compaction factor, i.e.,

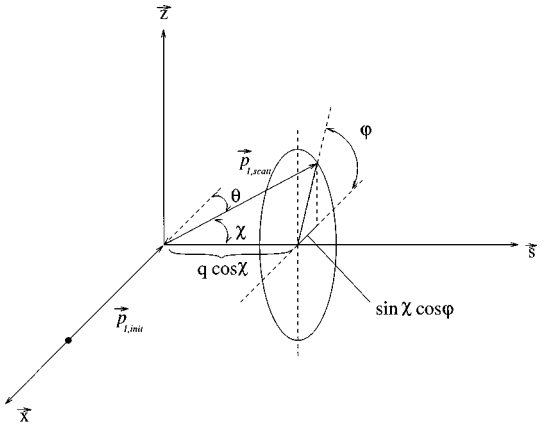

FIG. 11. The schematic geometry of Touschek scattering, which transfers horizontal momentum into the longitudinal momentum in the center of mass frame of collision particles. We use $\vec{x},\vec{s}$, and $\vec{z}$ as three orthonormal curvilinear coordinate system. Particle loss resulting from the large angle Coulomb scattering gives rise to the Touschek lifetime, which becomes a limiting factor for high brightness electron storage rings.

$$\frac{\widehat{\Delta p}}{p_0}=\left|\frac{\eta_0}{\eta_1}\right|. \tag{47}$$

This section examines the scaling property of the Touschek effect in the QI dynamical system.

We consider the Coulomb scattering of two particles in their center of mass system (CMS) with momentum $\vec{p}_{1,\mathrm{init}}=(p_x,0,0)$ and $\vec{p}_{2,\mathrm{init}}=(-p_x,0,0)$. Here the components of momentum vectors in $\hat{x},\hat{s}$, and $\hat{z}$ base vectors are specified. Since the transverse radial momentum component of the orbiting particle is much larger than the transverse vertical and the longitudinal components, we assume that the initial particle momenta of scattering particles are only in the horizontal direction. curvilinear coordinate system. After the collision, each particle is scattered by an angle θ. The differential cross section is given by the Möller formula

$$\frac{d\sigma}{d\Omega}=\frac{4r_0^2}{(v/c)^4}\left[\frac{4}{\sin^4\theta}-\frac{3}{\sin^2\theta}\right], \tag{48}$$

where r_0 is the classical electron radius, and $v=2p_x/m$ is the relative velocity in the CMS. As shown in Fig. 11, let χ be the angle between the momentum $\vec{p}_{1,\mathrm{scatt}}$ of a scattered particle and the s axis, φ be the angle between the x axis and the projection of the momentum of the scattered particle onto the x-z plane. Using the geometry shown in Fig. 11, the momentum of a scattered particle is given by

$$\vec{p}_{1,\mathrm{scatt}}=(p_x\sin\chi\cos\varphi,p_x\cos\chi,p_x\sin\chi\sin\varphi), \tag{49}$$

and the momentum of the other scattered particle is $-\vec{p}_{1,\mathrm{scatt}}$. The scattering angle θ is related to the χ and φ by

$$\cos\theta=\sin\chi\cos\varphi, \tag{50}$$

and the momentum transfer to the longitudinal plane in the CMS is given by

$$\Delta p_c = p_x |\cos\chi|. \tag{51}$$

Now we assume that the scattered particles will be lost if the scattered longitudinal momentum is larger than the momentum aperture, i.e.,

$$|\cos\chi| \geqslant \frac{\Delta\hat{p}}{\gamma p_x} = \frac{p_0|\eta_0|}{\gamma|\eta_1|p_x}. \tag{52}$$

Thus the total cross section leading to particle loss in the CMS is given by

$$\begin{aligned}\sigma_{\mathrm{T}} &= \int_{|\cos\chi| \geqslant \Delta\hat{p}/\gamma p_x} d\sigma \\ &= \frac{4r_0^2}{(v/c)^4}\int_0^{\arccos(\Delta\hat{p}/\gamma p_x)} \sin\chi d\chi \int_0^{2\pi} d\varphi \left[\frac{4}{(1-\sin^2\chi\cos^2\varphi)^2} - \frac{3}{(1-\sin^2\chi\cos^2\varphi)}\right] \\ &= \frac{8\pi r_0^2}{(v/c)^4}\left[\frac{\gamma^2 p_x^2}{(\Delta\hat{p})^2} - 1 + \ln\frac{\Delta\hat{p}}{\gamma p_x}\right].\end{aligned} \tag{53}$$

The number of particle loss due to the Touschek scattering in the CMS becomes

$$dN = 2\sigma_{\mathrm{T}} N n\, dx, \tag{54}$$

where n is the density of the beam bunch, $n\,dx$ is the target thickness, N is the total number of particles in the bunch, and the factor of 2 depicts the fact that two particles are lost in each Touschek scattering. Thus the lost rate in the CMS is given by $dN/dt = 2\int \sigma_{\mathrm{T}} v n^2 dV$, where dV is the volume element, and $v = dx/dt$.

In the laboratory frame, the Touschek loss rate becomes

$$\frac{dN}{dt} = \frac{2}{\gamma^2}\int v\sigma_{\mathrm{T}} n^2 dV, \tag{55}$$

where the $1/\gamma^2$ factor takes into account the Lorentz transformation of $\sigma_{\mathrm{T}} v$ from the CMS to the laboratory frame. Since the Touschek scattering takes place only in the horizontal plane, the vertical and the longitudinal planes can be integrated easily, and the Touschek loss rate becomes

$$\frac{dN}{dt} = 2\frac{N^2}{\gamma^2}\frac{1}{4\pi\sigma_z\sigma_s}\int v\sigma_{\mathrm{T}}\rho(x_1,x_1')\rho(x_2,x_2')\delta(x_1-x_2) \times dx_1 dx_1' dx_2 dx_2', \tag{56}$$

where σ_z and σ_s are, respectively, the rms bunch height and bunch length, the $\delta(x_1-x_2)$ function describes the fact that the scattering process takes place at a short range between two particles, and the density function of the beam is given by

$$\rho(x,x') = \frac{\beta_x}{2\pi\sigma_x^2}\exp\left\{-\left[x^2 + \left(\beta_x x' - \frac{\beta_x'}{2}x\right)^2\right] \Big/ 2\sigma_x^2\right\}. \tag{57}$$

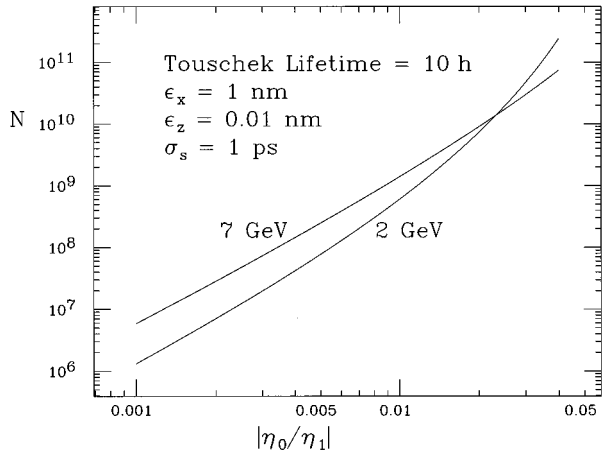

FIG. 12. The expected number of particles per bunch in the QI storage ring limited by the Touschek lifetime of 10 h for electron beam energy of 2 GeV and 7 GeV, respectively. The assumed parameters are $\tau_{\mathrm{T}} = 10$ h, $\sigma_s = 1$ ps, and unnormalized rms emittances $\epsilon_x = 1$ nm, $\epsilon_z = 0.01$ nm, with typical betatron amplitude functions of 10 m.

The integral can be integrated easily to obtain

$$\frac{1}{N}\frac{dN}{dt} = \frac{1}{\tau_{\mathrm{T}}} = \frac{Nr_0^2 c}{8\gamma^2\pi\sigma_x\sigma_z\sigma_s}\left|\frac{\eta_1}{\eta_0}\right|^3 D(\xi), \tag{58}$$

where

$$D(\xi) = \sqrt{\xi}\left[-\frac{3}{2}e^{-\xi} + \frac{\xi}{2}\int_\xi^\infty \frac{\ln u}{u}e^{-u}du + \frac{1}{2}(2+3\xi-\xi\ln\xi)\int_\xi^\infty \frac{e^{-u}}{u}du\right] \tag{59}$$

with

$$\xi = \left(\frac{\Delta\hat{p}}{\gamma\sigma_p}\right)^2 = \left(\frac{|\eta_0|}{\gamma\sigma_p|\eta_1|}\right)^2$$

and

$$\sigma_p = \frac{\gamma mc\sigma_x}{\beta_x}.$$

Figure 12 shows the maximum bunch intensity as a function of $|\eta_0/\eta_1|$ with beam parameters given by $\tau_{\mathrm{T}} = 10$ h, $\sigma_s = 1$ ps and unnormalized rms emittances $\epsilon_x = 1$ nm, $\epsilon_z = 0.01$ nm, with typical betatron amplitude functions of 10 m. For other possible parameters, the tolerable beam intensity can be scaled accordingly. Note that the tolerable number of particles in QI storage rings depends sensitively on the ratio $|\eta_0/\eta_1|$. As $|\eta_0| \to 0$ in QI storage rings, a proper η_1 correction is needed, where sextupoles can be used.

V. CONCLUSION

The equilibrium distribution function obtained from the Fokker-Planck equation arising from white noise and phase space damping depends solely on the unperturbed Hamiltonian, i.e., the distortion of the Hamiltonian contour due to

phase space damping is balanced by the quantum fluctuation. The bunch size is determined by a single parameter $E_{\rm th}=D^2/2A$, where D is the quantum fluctuation amplitude and A is the effective damping parameter. Both the normalized damping parameter A and the quantum diffusion parameter D are enhanced; and at the same time, the thermal energy $E_{\rm th}$ of the beam is also enhanced. The distribution function in the momentum coordinate is non-Gaussian due to anharmonicity in the QI Hamiltonian unless the thermal energy is much smaller than the separatrix energy.

Because the effective damping parameter for QI dynamical systems is enhanced, the quantum lifetime can only be described by the BHL formula. The conventional expression used in accelerator physics may greatly underestimate the actual quantum lifetime. The effects of the potential well distortion due to the wake field of the beam bunch are found to be identical to that of the normal rf system. Furthermore, we derive formula of the Touschek lifetime for the QI electron storage rings. The necessary condition for the $|\eta_1|$ correction in order to attain high beam intensity in QI storage rings is calculated.

When the harmonic rf phase modulation is applied to the QI stochastic dynamical system, the cusp in the stability diagram shown in Ref. [3] is smoothed by the quantum fluctuation. Yet, particles still damp incoherently to bunches around attractors (SFPs) with the same thermal energy parameter $E_{\rm th}$. These attractors rotate about the center of the bucket at the modulation frequency. The reduced quantum lifetime can be explained by the fact that the effective potential energy difference between the SFP and the top of the potential barrier is reduced by the rf phase modulation. In particular, we show that the stochastic resonance, a phenomenon of periodically enhanced quantum tunneling (decay) rate at a low modulation frequency, can be unambiguously quantitatively identified as due to the 1:1 parametric resonance.

ACKNOWLEDGMENTS

The work was supported in part by grants from the DOE-DE-FG02-93ER40801 and NSF PHY-9512832 We thank C.M. Chu and X. Kang for their help in calculations.

APPENDIX A: BRIEF REVIEW OF THE QI DYNAMICAL SYSTEM

The equation of motion for the rf phase coordinate ϕ of a particle in a synchrotron is given by

$$\dot{\phi}=h\eta\delta, \tag{A1}$$

where h is the harmonic number, $\delta=\Delta p/p$ is the fractional momentum deviation from the synchronous particle, the overdot is the derivative with respect to the orbiting angle $\theta=s/R_0$, and η is the phase slip factor given by

$$\eta=\eta_0+\eta_1\delta+\cdots, \tag{A2}$$

where η_0 and η_1 are the first order and the second order phase slip factors. In many realistic storage rings, the truncation of the phase slip factor at the η_1 term is a good approximation. Similarly, the equation of motion for the fractional off-momentum deviation is given by

$$\dot{\delta}=\frac{eV_0}{2\pi\beta^2E_0}[\sin(\phi+\phi_s)-\sin\phi_s], \tag{A3}$$

where V_0 and ϕ_s are the rf voltage and the synchronous phase angle, and βc and E_0 are the velocity and the energy of the beam.

Using $t=\nu_s\theta$ as the time variable, where $\nu_s=\sqrt{he V_0|\eta_0\cos\phi_s|/2\pi\beta^2E_0}$ is the small amplitude synchrotron tune, and using (x,p) as conjugate phase space coordinates, where

$$x=-\frac{\eta_1}{\eta_0}\frac{\Delta p}{p_0},\quad p=\frac{\nu_s\eta_1}{h\eta_0^2}\phi, \tag{A4}$$

the synchrotron Hamiltonian for particle motion in QI storage rings is given by [2]

$$H_0=\frac{1}{2}p^2+\frac{1}{2}x^2-\frac{1}{3}x^3. \tag{A5}$$

Since the universal Hamiltonian is autonomous, the ''energy'' E is a constant of motion. For particles inside the bucket, $E\in[0,\frac{1}{6}]$.

The equation of motion in QI Hamiltonian with energy E is given by the standard Weierstrass equation:

$$\left(\frac{d\wp(u)}{du}\right)^2=4(\wp-e_1)(\wp-e_2)(\wp-e_3), \tag{A6}$$

where $u=(1/\sqrt{6})t$, $\wp=x$, and turning points are given by $e_1=\frac{1}{2}+\cos(\xi)$, $e_2=\frac{1}{2}+\cos(\xi-120°)$, $e_3=\frac{1}{2}+\cos(\xi+120°)$, with $\xi=\frac{1}{3}\arccos(1-12E)$.

The Weierstrass elliptic $\wp$ function is a single valued doubly periodic function of a single complex variable. For particle inside the separatrix, the discriminant $\Delta=648E(1-6E)$ is positive, and the Weierstrass $\wp$ function can be expressed in terms of the Jacobian elliptic function [6]

$$x(t)=e_3+(e_2-e_3)\mathrm{sn}^2\left(\sqrt{\frac{e_1-e_3}{6}}t\,\middle|\,m\right), \tag{A7}$$

$$m=\frac{e_2-e_3}{e_1-e_3}=\frac{\sin\xi}{\sin(\xi+60°)}. \tag{A8}$$

The separatrix orbit, which corresponds to $m=1$, is given by

$$x_{sx}(t)=1-\frac{3}{\cosh t+1},\quad p_{sx}(t)=\frac{3\sinh t}{(\cosh t+1)^2}. \tag{A9}$$

The tune of the QI Hamiltonian is given by

$$Q(E)=\frac{\pi[\sqrt{3}\sin(\xi+60°)]^{1/2}}{\sqrt{6}K(m)}. \tag{A10}$$

We note particularly that the synchrotron tune decreases to zero very sharply near the separatrix. Because of the sharp decrease in synchrotron tune, time dependent perturbation will cause overlapping parametric resonances and chaos near the separatrix [17–19]. The action of a torus is given by

$$J=\frac{1}{2\pi}\oint p\,dx=\frac{1}{8}\sqrt{\frac{2}{3}}(e_2-e_3)^2(e_1-e_3)^{1/2}F\left(\frac{3}{2},-\frac{1}{2};3;m\right), \tag{A11}$$

where F is the hypergeometric function [6]. The separatrix action is given by $J_{sx}=3/5\pi$. Using the generating function

$$F_2(x,J)=\int_{e_3}^{x}p\,dx, \tag{A12}$$

the angle variable is given by $\psi=\partial F_2/\partial J=Qt$. The resulting Hamiltonian is given by

$$H_0(J)\approx J-\frac{5}{12}J^2+\cdots.$$

Due to the synchrotron radiation damping, the equation of motion for QI storage rings is given by

$$x''+Ax'+x-x^2=0, \tag{A13}$$

where the effective damping coefficient is given by

$$A=\frac{\lambda}{\nu_s}=\frac{U_0J_E}{2\pi E_0\nu_s}. \tag{A14}$$

Here λ is the damping decrement, U_0 is the energy loss per revolution, and J_E is the damping partition number. In QI storage rings, the effective damping coefficient is enhanced by the corresponding decrease in the synchrotron tune, i.e., $A\sim|\eta_0|^{-1/2}$, where the value of A can vary from 0 to 0.5.

Including the rf phase noise, the Hamiltonian in the normalized phase space coordinates is given by

$$H=\frac{p^2}{2}+\frac{1}{2}x^2-\frac{1}{3}x^3+\omega_mBx\cos\omega_mt, \tag{A15}$$

where $\omega_m=\nu_m/\nu_s$ is the normalized modulation tune, and a and ν_m are, respectively, the rf phase modulation amplitude and the modulation tune in the original accelerator coordinate system. Note that the effective modulation amplitude given by

$$B=\frac{\eta_1 a}{\eta_0\nu_s} \tag{A16}$$

is greatly enhanced for QI storage rings, i.e., $B\sim|\eta_1|/|\eta_0|^{3/2}$. Including the damping force, the equation of motion becomes

$$x''+Ax'+x-x^2=-\omega_mB\cos\omega_mt. \tag{A17}$$

APPENDIX B: ALGORITHM FOR STOCHASTIC INTEGRATION

Electrons in storage rings emit synchrotron radiation, which is a quantum process. Since the photon emission is discrete and random, the quantum process causes also diffusion and excitation. The balance between the damping and excitation provides a natural emittance or beam size for the electron beam bunch in storage rings. Because of the synchrotron radiation spectrum depends weakly on the energy of photons up to the critical frequency, the emission of photons can be approximated by white noise, i.e., electrons are acted on a Langevin force. To solve the resulting stochastic differential equation numerically, we examined several numerical algorithms in this appendix.

1. Random walk method

Including the quantum emission of photons, the difference equation for the normalized synchrotron phase space coordinates is given by

$$x_{i+1}=x_i+2\pi\nu_s(-Ax_i+p_i), \tag{B1}$$

$$p_{i+1}=p_i+2\pi\nu_s(-x_{i+1}+x_{i+1}^2)+(2\pi\nu_s)^{1/2}DW(t), \tag{B2}$$

where the subscript depicts the revolution number, and ν_s is the synchrotron tune. The Wiener process function $W(t)$ is defined by

$$W(t)=\frac{1}{T_0^{1/2}}\int_t^{t+T_0}\xi(t')dt', \tag{B3}$$

where T_0 is the time for one revolution in the ring, and the white-noise function, denoted by $\xi(t)$, has the properties:

$$\langle\xi(t)\rangle=0,\quad \langle\xi(t)\xi(t')\rangle=\delta(t-t'). \tag{B4}$$

Thus the variance of the Wiener process function becomes

$$\langle W(t)W(t)\rangle=1. \tag{B5}$$

Therefore in the tracking equations of Eq. (B2), a Wiener process $W(t)$ can be imitated by a random walk of ±1 per revolution. In the smooth approximation, Eq. (B2) is equivalent to the differential equations of motion:

$$\frac{dx}{dt}=-\left(\frac{2\pi\nu_s}{T_0}\right)Ax+\left(\frac{2\pi\nu_s}{T_0}\right)p, \tag{B6}$$

$$\frac{dp}{dt}=\left(\frac{2\pi\nu_s}{T_0}\right)(-x+x^2)+\left(\frac{2\pi\nu_s}{T_0}\right)^{1/2}D\xi(t). \tag{B7}$$

Here t is the real time for the particle motion in a storage ring.

2. Stochastic integration methods

For one stochastic variable x, the general Langevin equation has the form

$$\dot{x}(t)=f(x)+g(x)\xi(t). \tag{B8}$$

The Langevin force $\xi(t)$ is assumed to be a Gaussian random variable with zero mean and δ-function correlation shown in Eq. (B4). The integration of Eq. (B8) is given by

$$x(t+h)=x(t)+f(x)h+g(x)\sqrt{h}W(h), \tag{B9}$$

where

$$W(h)=\frac{1}{\sqrt{h}}\int_t^{t+h}ds\,\xi(s).$$

Two widely used methods for solving stochastic differential equations numerically are presented below.

a. Euler's scheme

This integration scheme includes terms up to the order h for additive noise. To integrate stochastic differential equations from $t=0$ to $t=T$, we first divide the time interval T into N small finite steps of length h

$$t_n=nh, \quad h=T/N, \quad n=1,2,\ldots,N.$$

The stochastic variable at a later time t_{n+1}

$$x_{n+1}=x(t_{n+1})=x((n+1)h) \tag{B10}$$

is calculated according to

$$x_{n+1}=x_n+f(x_n)h+g(x_n)\sqrt{h}W_n(h), \tag{B11}$$

where $W_1(h)$, $W_2(h),\ldots,$ $W_N(h)$ are independent Gaussian-distributed random variables with zero mean and variance 1, i.e.,

$$\langle W_n\rangle=0, \quad \langle W_nW_m\rangle=\delta_{nm}. \tag{B12}$$

A possible choice of the set of Gaussian random variable W_n is given by

$$W_n(h)=\sum_{i=1}^{M}\sqrt{\frac{12}{M}}(r_i-0.5), \tag{B13}$$

where r_i is a random number with $0\leqslant r_i<1$, and M is an arbitrary nonzero large integer, e.g., $M\geqslant 10$.

b. Heun's scheme

Heun's scheme is of second order in h. The difference from the Euler's scheme is an additional predictor step.

$$x_{n+1}=x_n+\frac{1}{2}[f(x_n)+f(y_n)]h+g(x_n)\sqrt{h}W_{2n-1}(h) \tag{B14}$$

with

$$y_n=x_n+f(x_n)h+g(x_n)\sqrt{h}W_{2n}(h).$$

In this case we need $2N$ independent random variables $\{W_n(h)\}$. The equilibrium distribution function does not depend on the method of stochastic integration used in numerical simulations. It is, however, worth pointing out that a nonsymplectic integration method can lead to a slightly different $E_{\rm th}$ due essentially to the change in the effective A parameter.

APPENDIX C: VIRIAL THEOREM

We consider a stochastic Hamiltonian $H(p,q)$, where (p,q) are conjugate phase space coordinates. We are interested in the ensemble average of such a system, which is denoted by $\langle\cdots\rangle$. In particular, at an ''energy'' E, we have

$$\left\langle p\frac{\partial H}{\partial p}\right\rangle_E=\frac{1}{\Gamma(E)}\int_{E<H<E+\Delta}dpdq\left(p\frac{\partial H}{\partial p}\right), \tag{C1}$$

where

$$\Gamma(E)=\frac{\partial\Sigma}{\partial E}\Delta \tag{C2}$$

is the phase space area in the infinitesimal energy shell $E<H<E+\Delta$ with an infinitesimal parameter Δ, and $\Sigma(E)$ is the phase space area for $H<E$. The integration over the thin energy shell of thickness Δ can be converted into a differentiation

$$\begin{aligned}\left\langle p\frac{\partial H}{\partial p}\right\rangle_E&=\frac{\Delta}{\Gamma(E)}\frac{\partial}{\partial E}\int_{H<E}dpdq\left(p\frac{\partial(H-E)}{\partial p}\right)\\&=\frac{\Delta}{\Gamma(E)}\frac{\partial}{\partial E}\int_{H<E}dpdq\left\{\frac{\partial}{\partial p}[p(H-E)]-(H-E)\right\}.\end{aligned} \tag{C3}$$

Here E is a constant. The first term integrates to zero on the boundary $H=E$, while the second term gives

$$\begin{aligned}\left\langle p\frac{\partial H}{\partial p}\right\rangle_E&=\frac{\Delta}{\Gamma(E)}\int_{H<E}dpdq\\&\quad-\frac{1}{\Gamma(E)}\int_{E<H<E+\Delta}dpdq(H-E).\end{aligned} \tag{C4}$$

Using the mean value theorem, we find, in the limit of $\Delta\to 0$,

$$\begin{aligned}&-\frac{1}{\Gamma(E)}\int_{E<H<E+\Delta}dpdq(H-E)\\&=-\frac{\xi\Delta}{\Gamma(E)}\int_{E<H<E+\Delta}dpdq\\&=-\xi\Delta\to 0,\end{aligned} \tag{C5}$$

where ξ is a number between 0 and 1. Thus, we finally arrive at

$$\left\langle p\frac{\partial H}{\partial p}\right\rangle_E=\frac{\Sigma(E)}{\partial\Sigma(E)/\partial E}. \tag{C6}$$

Similarly, we find also

$$\left\langle q\frac{\partial H}{\partial q}\right\rangle_E=\frac{\Sigma(E)}{\partial\Sigma(E)/\partial E}, \tag{C7}$$

and

$$\left\langle\frac{\partial H}{\partial p}\right\rangle_E=\left\langle\frac{\partial H}{\partial q}\right\rangle_E=0. \tag{C8}$$

For the QI Hamiltonian with $H=\frac{1}{2}p^2+\frac{1}{2}x^2-\frac{1}{3}x^3$, we get

$$\langle p\rangle = 0,$$

$$\langle p^2\rangle = \langle x^2\rangle - \langle x^3\rangle,$$

$$\langle x\rangle = \langle x^2\rangle,$$

where the subscript E has been omitted. We thus obtain

$$\left\langle \tfrac{1}{2}\, p^2\right\rangle = \tfrac{1}{2}\langle H\rangle - \tfrac{1}{12}\langle x^3\rangle, \tag{C9}$$

$$\left\langle \tfrac{1}{2}\, x^2 - \tfrac{1}{3}x^3\right\rangle = \tfrac{1}{2}\langle H\rangle + \tfrac{1}{12}\langle x^3\rangle. \tag{C10}$$

Since $\langle x^3\rangle/12$ is small, we obtain an approximate equipartition theorem for the QI Hamiltonian.

[1] *Micro Bunches Workshop*, edited by E. B. Blum, M. Dienes, and J. B. Murphy, AIP Conference Proceedings No. 367 (AIP, New York, 1996).

[2] A. Riabko *et al.*, Phys. Rev. E **54**, 806 (1996).

[3] D. Jeon *et al.*, Phys. Rev. E **54**, 4192 (1996).

[4] C. Pelligrini and D. Robin, Nucl. Instrum. Methods A **301**, 27 (1991); D. Robin, E. Forest, C. Pelligrini, and A. Amiry, Phys. Rev. E **48**, 2149 (1993); L. Liu *et al.*, Nucl. Instrum. Methods A **329**, 9 (1993); H. Hama, S. Takano, and B. Isoyoma, *ibid.* **329**, 29 (1993); S. Takano, H. Hama, and G. Isoyama, Jpn. J. Appl. Phys. **32**, 1285 (1993); D. Robin, H. Hama, and A. Nadji, in *Micro Bunches Workshop* (Ref. [1]), p. 150; D. Robin *et al.*, *Micro Bunches Workshop* (Ref. [1]), p. 181.

[5] D.F. Lawden, *Elliptic Functions and Applications*, Applied Mathematical Sciences Vol. 80, (Springer-Verlag, New York, 1989).

[6] *Handbook of Mathematical Functions*, edited by M. Abramowitz and I.A. Stegun (National Bureau of Standards, Washington, D.C., 1975).

[7] M.H. Devoret *et al.*, Phys. Rev. B **36**, 58 (1987).

[8] P. Jung and P. Hanggi, Phys. Rev. A **41**, 2977 (1990).

[9] H. Risken, *The Fokker-Planck Equation*, 2nd ed. (Springer-Verlag, New York, 1989).

[10] A. Gerasimov and S.Y. Lee, Phys. Rev. E **49**, 3881 (1994).

[11] M. Büttiker, E.P. Harris, and R. Landerauer, Phys. Rev. B **28**, 1268 (1983).

[12] H.A. Kramers, Physica (Utrecht) **7**, 284 (1940).

[13] S. Chandrasekhar, Rev. Mod. Phys. **15**, 1 (1943).

[14] J. Haissinski, Nuovo Cimento **18B**, 72 (1973).

[15] A.W. Chao, *Physics of collective beam instabilities in high energy accelerators* (John Wiley & Sons, Inc., New York, 1993).

[16] S. Matsumoto, in *Micro Bunches Workshop* (Ref. [1]), p. 455.

[17] S.Y. Lee *et al.*, Phys. Rev. E **49**, 5717 (1994); J.Y. Liu *et al.*, *ibid.* **50**, R3349 (1994); Part. Accel. **49**, 221 (1995).

[18] D. Li *et al.*, Phys. Rev. E **48**, R1638 (1993); Nucl. Instrum. Methods A **364**, 205 (1995).

[19] H. Huang *et al.*, Phys. Rev. E **48**, 4678 (1993); M. Ellison *et al.*, Phys. Rev. Lett. **70**, 591 (1993); M. Syphers *et al.*, *ibid.* **71**, 719 (1993); Y. Wang *et al.*, Phys. Rev. E **49**, 1610 (1994).

[20] L.D. Landau and E.M. Lifshitz, *Mechanics*, 2nd ed. (Oxford, New York, 1969).

[21] C. Bernardini *et al.*, Phys. Rev. Lett. **10**, 407 (1963).